Organic Electronics 13 (2012) 53–57

Contents lists available at SciVerse ScienceDirect

Organic Electronics

journal homepage: www.elsevier.com/locate/orgel

Silica nanoparticle-embedded sol–gel organic/inorganic hybrid nanocomposite for transparent OLED encapsulation

Jungho Jin [a], Jae Jun Lee [a], Byeong-Soo Bae [a,*], Soo Jin Park [b], Seunghyup Yoo [b], KyungHo Jung [c]

[a] Department of Materials Science and Engineering, KAIST, Daejeon 305-701, Republic of Korea
[b] Department of Electrical Engineering, KAIST, Daejeon 305-701, Republic of Korea
[c] Nano Technology Group, Future Device R&D Lab., Advanced Research Institute of LG Electronics Inc., Seoul, Republic of Korea

ARTICLE INFO

Article history:
Received 29 July 2011
Received in revised form 1 September 2011
Accepted 18 September 2011
Available online 11 October 2011

Keywords:
Gas barrier layer
Silica nanoparticle
Sol–gel
Hybrid nanocomposite
OLED encapsulation
Ca-test

ABSTRACT

We report a transparent moisture barrier coating fabricated with a silica nanoparticle-embedded organic/inorganic hybrid (S–H) nanocomposite. We used a photo-curable, cyclo-aliphatic epoxy based hybrid material (hyrimer) as the matrix and a solvent-less, monodisperse silica nanoparticles as the reinforcement responsible for creating tortuous diffusive path for moisture penetrants. The S–H nanocomposite barrier coating exhibits a single layer WVTR of 0.24 g/m^2 day (Ca-test) and an optical transparency of 90% in the visible range. The performance of the barrier coating was also verified in an OLED lifetime measurement test, in which an OLED encapsulated with an S–H nanocomposite barrier coating showed significantly extended lifetime.

1. Introduction

With the rapid development of organic light emitting diodes (OLEDs) as next-generation display/lighting devices, high-performance gas barrier coating has emerged as one of the most important component as the infiltration of moisture/oxygen gases significantly affects the shelf-life and quality of OLEDs [1]. The penetration of moisture/oxygen gases generally causes undesired oxidization or crystallization of organic layers, which accelerates the formation of dark non-emissive spots that seriously degrade the performance of OLEDs [2]. In particular, gas barrier coating on a plastic substrate has been studied intensively in relation to the development of flexible organic electronics. Thus, a gas barrier coating should provide not only a reliable gas barrier property, but also optical transparency and flexibility for practical display applications.

Several methods based on mass spectroscopy or coulometric sensing techniques (MOCON®) have been used to evaluate the gas permeability of barrier coatings. Particularly, the Ca-test has been widely used to examine the gas barrier property; it measures the water vapor transmission rate (WVTR) [3]. Typically required WVTR value for OLED barrier is of 10^{-5}–10^{-6} g/m^2 day (10^{-2} g/m^2 day for LCDs).

Vacuum-deposited inorganic thin films, such as Al_2O_3, SiO_x, and Si_3N_4, are reported to exhibit excellent barrier properties and thus are widely used in OLED barrier layers [4]. However, they often produce defects such as pinholes and cracks, particularly when deposited as a thin film on a plastic substrate. These defects can act as a direct propagation channel for gas penetrants, which in turn leads to inadequate WVTR values. Polymer/inorganic hybrid multi-stacks (dyads) have been introduced and used as high-performance gas barrier systems for the purpose of decoupling such defects and suppressing the channel effect [5]. However, the overall fabrication process for the multi-stacks is rather complicated and time-consuming. Thus, the development of materials which possess superior gas barrier properties as well as optical transparency and flexibility is crucial for effective encapsulation of OLEDs.

* Corresponding author.
E-mail address: bsbae@kaist.ac.kr (B.-S. Bae).

1566-1199/$ - see front matter © 2011 Elsevier B.V. All rights reserved.
doi:10.1016/j.orgel.2011.09.008

The design of effective gas barrier materials should be based on consideration of factors such as the density of the material, the existence of chemically reactive groups, hydrophobicity and the incorporation of nanofillers. In particular, polymer nanocomposites embedded with inorganic particles (such as clays) have been studied intensively for the purpose of improving the gas barrier properties [6]. The way nanofillers in a polymeric matrix affect the gas barrier properties have been well explicated by the tortuous path model (or Nelson's model) [7]. According to this model, the enhancement of the gas barrier properties is mainly attributed to an extended diffusive path, since the gas penetrants must detour around the fillers within the matrix. In this case, the gas barrier properties of a nanocomposite can be significantly affected by the degree of dispersion, the aspect ratio of the nanofillers and the dispersion morphology. Hence, the fabrication of nanocomposite barrier coatings with a homogeneous dispersion of nanofillers is essential for two reasons: (1) to effectively enhance the gas barrier properties and, (2) to ensure a high level of transparency of the barrier coating.

We previously reported on a novel organic/inorganic hybrid barrier coating which exhibited a single layer gas permeability of ~0.68 g/m^2 day (mil^{-1}) and an optical transparency level of ~90% in the visible region [8]. The hybrid barrier coating can be prepared via UV-induced polymerization of a sol–gel derived cyclo-aliphatic epoxy oligosiloxane resin (hybrimer) [9]. A demonstration of a subsequent lifetime measurement of an OLED encapsulated with a hybrimer barrier coating revealed that the lifetime of an OLED can be extended considerably in comparison with an uncapped device. In this study, we demonstrate a new type of moisture barrier coating based on silica nanoparticle-embedded hybrimer (S–H) nanocomposites, which exhibits enhanced barrier properties. The morphology of S–H nanocomposites was characterized with the aid of dynamic light scattering (DLS). The permeability values (WVTRs) of the S–H nanocomposite barrier coatings were then assessed in a Ca-test. Finally, we demonstrated the extended lifetime of an OLED encapsulated with an optimized barrier coating.

2. Materials and methods

The cyclo-aliphatic epoxy oligosiloxane resin (Fig. 1) was synthesized via a sol–gel reaction of 2-(3,4-epoxycyclohexyl) ethyl trimethoxysilane (ECTS) and diphenylsilanediol (DPSD). First, ECTS was mixed with $Ba(OH)_2{\cdot}H_2O$, the catalyst for the sol–gel reaction, and the mixture was reacted with DPSD in a two-neck flask at 80 °C under N_2 purging for 4 h. Molar ratio of MPTS to DPSD was fixed at 2:3. After the reaction, a viscous, colorless resin was obtained. The resin was then mixed with arylsulfonium hexafluorophosphate salt (2 wt%) which is the catalyst for photo-cationic polymerization. The basic structural characterization are described in our previous works [8].

For the S–H nanocomposites, we used Nanopox® E600 (Nanoresins, Germany) which consists of solvent-less, methyl-terminated silica nanoparticles dispersed in a reactive diluent of 3,4-epoxycyclohexyl methyl 3,4-epoxycyclohexane carboxylate (EMEC) (Fig. 1). Nanopox® E600 alone was unable to be fully UV-cured within a certain period of time and, moreover, it showed a poor coating quality with undesired pores due to its severe shrinkage. Nonetheless, we hypothesized that, by using Nanopox® E600, the dispersion of silica nanoparticles in the oligosiloxane resin would be advantageous in terms of molecular affinity because of the cyclo-aliphatic epoxy oligosiloxane groups in the Nanopox® E600. In fact, the cyclo-aliphatic epoxy oligosiloxane resin and EMEC form a homogeneous, co-polymerizable blend. However, we found that this hypothesis fails in S–H nanocomposites that have low silica content. We used a conditioning paste mixer to mix

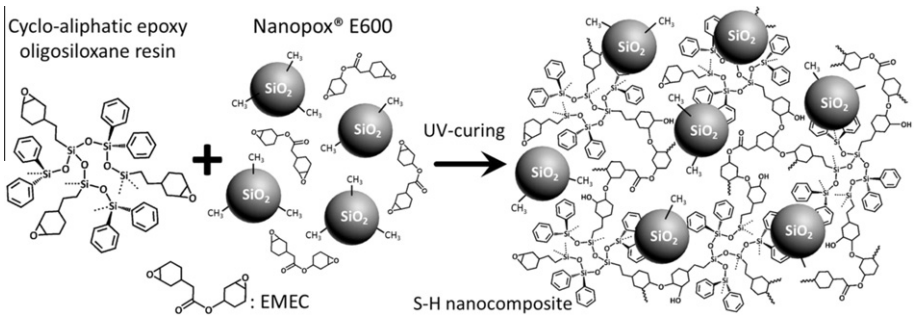

Fig. 1. S–H nanocomposite fabricated with a sol–gel cycloaliphatic oligosiloxane resin and Nanopox® E600.

Table 1
Resin formulation for S–H nanocomposites and WVTR values of S–H nanocomposites barrier coatings on PET film.

	Silica content (wt%)	Oligosiloxane resin (g)	Nanopox® E600 (g)	Thickness (μm)	WVTR (g/m^2 day)
Hybrimer	0	10	0	4	3.90
S–H nano-composites	10	10	2.5		3.56
	25	10	6.25		1.80
	50	10	12.5		0.90
	100	10	25		0.24
PET	–	–	–	100	24.4

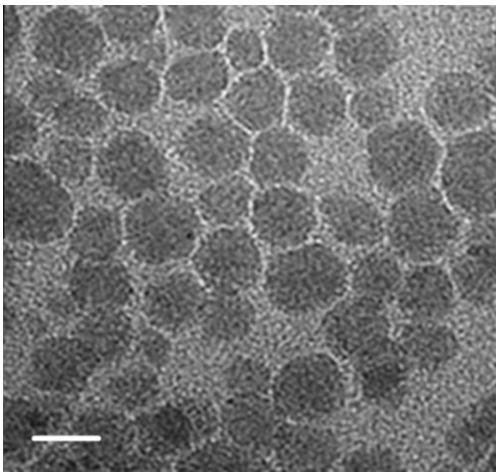

Fig. 2. TEM image of the S–H nanocomposite (100 wt% silica). The inset scale bar represent 20 nm.

various amounts of Nanopox® E600 with the oligosiloxane resin – the total silica content in the oligosiloxane resin was varied from 10, 25, 50, and 100 wt%. Because the solid content of Nanopox® E600 is ~40%, we precisely formulated the S–H nanocomposite resins with different amounts of silica based on the compositions listed in Table 1. Propylene glycol monoether acetate was then added as a diluent for the coating and mixed with a magnetic stirrer for 30 min. To ensure a homogeneous dispersion of silica nanoparticles, we sonicated the mixed resins for another 30 min. Finally, the S–H nanocomposite resins were spin-coated on a 100 μm-thick PET film and subsequently UV-cured with an Hg-lamp (λ = 350–390 nm, 85 mW/cm^2). Fig. 2 shows a TEM image of the S–H nanocomposite with 100 wt% silica content. The thickness of all the S–H nanocomposite coatings was kept at 4 μm for the Ca-test and OLED lifetime measurement test. Detailed information on the fabrication and performance of the OLED as well as the basic experimental setup for both Ca-test and OLED lifetime measurement can be found in the ESM.

3. Results and discussion

3.1. Dispersion morphology of S–H nanocomposites

DLS analysis was used to determine the average particle size and dispersion morphology of S–H nanocomposites. As shown in the DLS spectra (Fig. 3), the average diameter of the embedded silica particles decreased from 127 nm (for a 10 wt% content) to 19 nm (for a 100 wt% content); the latter corresponds to the size of a single silica particle.

In Fig. 3, note the significant narrowing of the size distribution as the silica content is increased. These results indicate that, in samples with a low silica content (of 10 or 25 wt%), the embedded silica particles tend to exist as agglomerates with broad size variations and eventually become homogeneously dispersed when the silica content is increased (to 100 wt%).

In terms of thermodynamics, the agglomeration of silica nanoparticles in samples with a low silica content can be attributed to the fact that the enthalpic interactions between the oligosiloxane resin and the silica nanoparticles are more dominant than the entropic effect, thus the overall dispersion is unfavorable [10]. This behavior can be explicated by the fact that the organic surroundings of the two phases are heterogeneous (phenyl vs. methyl, as shown in Fig. 1); there is even high probability of oligosiloxane-nanoparticle contacts when the silica content is low. Moreover, the entropic effect is unlikely to be sufficiently dominant to favor a homogeneous dispersion because the size of silica particles greatly surpasses that of the oligosiloxanes [11]. When the silica content is increased, however, the enthalpic interactions become imperceptible, which allows a homogeneous dispersion even without any phase separation.

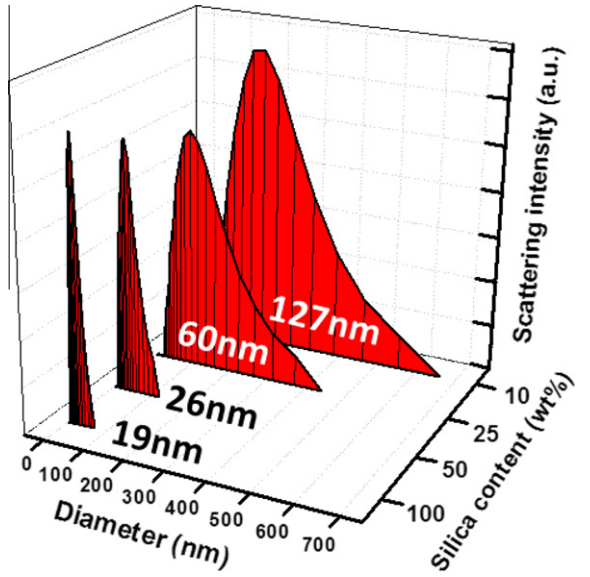

Fig. 3. DLS spectra of the S–H nanocomposites and the average particle diameters (inset numbers).

3.2. Optical property of S–H nanocomposites

The optical transparency of the S–H nanocomposite barrier coatings were characterized with an UV–vis spectrophotometer. In Fig. 4, note that all the S–H nanocomposite barrier coatings show transmittance level of over 90% regardless of silica content. However, there is a slight degradation of the transmittance in samples with low silica content (10 and 25 wt%). This tendency can be attributed to the sufficiently large particle agglomerates that are responsible for scattering of visible light as evidenced in the DLS spectra (Fig. 3).

3.3. Moisture barrier properties of S–H nanocomposites

The moisture barrier properties of S–H nanocomposite barrier coatings were characterized by a Ca-test (Fig. S1), and the performance of an optimized barrier coating was verified in a subsequent OLED lifetime measurement test. Detailed information on the basic experimental setup for both tests can be found in the ESM. Fig. 5 shows the Ca-test results of a single S–H nanocomposite barrier coating on a

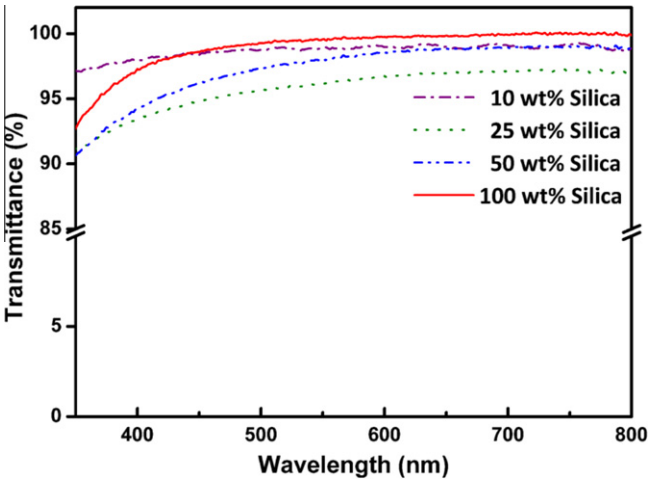

Fig. 4. UV–vis spectra of the S–H nanocomposite barrier coatings with different amounts of silica.

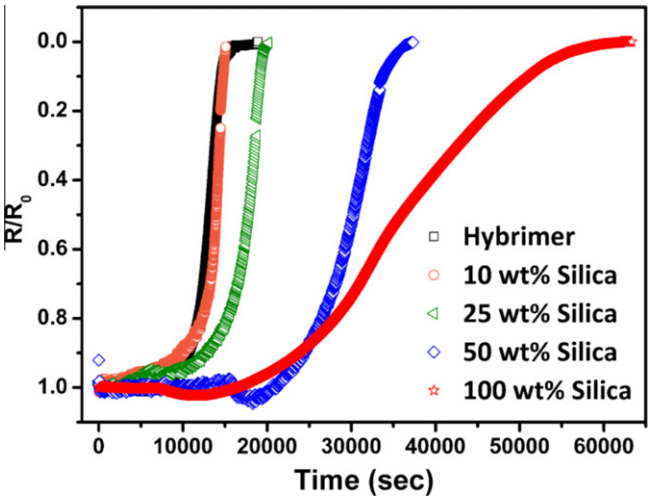

Fig. 5. Ca-test results of S–H nanocomposite barrier coatings with different silica contents (25 °C, >90% RH). Plots of normalized resistivity (R/R_0) vs. time.

PET film; the results are plotted as normalized resistivity (R/R_0) vs. time curves. Table 1 shows the WVTR values calculated from the slope of each curve. The S–H nanocomposite barrier coatings show that an increase in silica content leads to significant improvement in the WVTR values (that is, from 3.56 g/m^2 day for 10 wt% silica to 0.24 g/m^2 day for 100 wt% silica). On the basis of the tortuous path model, the enhanced moisture properties of S–H nanocomposites can be attributed to the extended diffusive path for water vapor penetrants. Note that such enhancements are more pronounced in samples with a high silica content (of 50 and of 100 wt%). This is in correlation between the overall density of the tortuous paths and the dispersion morphology.

The enhanced moisture barrier properties of the S–H nanocomposite was verified in a subsequent OLED lifetime measurement taken under the same conditions as the Ca-test (25 °C, >90% RH). We also measured the lifetime of an uncapped OLED and a PET-encapsulated OLED as references. For the OLED, we used *N*,*N*′-bis(naphthalen-1-yl)-*N*,*N*′-bis(phenyl)-benzidine (NPB) and tris(8-hydroxy-quinolinato) aluminum (Alq3) as the charge transporting and emitting organic layers, and LiF/Al as the cathode. Detailed information on the fabrication and performance of the OLED can be found in the ESM. Fig. 6(a) depicts the OLED structure as well as the test setup for the lifetime measurement test, and Fig. 6(b) shows an optical image of luminescence of the OLED encapsulated with the optimized S–H nanocomposite barrier coating. The point where the luminescence and applied voltage both fell 50% below their initial values marked the end of the lifetime. As shown in Fig. 6(c), the OLED lifetime measurements were 70 min for the uncapped case, 165 min for the bare PET case, 425 min for the neat hybrimer case, and 745 min for our optimized S–H nanocompoiste barrier coating (with 100 wt% silica); that is more than 10 times longer than the uncapped case. The considerable extension in the lifetime of the OLED encapsulated with the optimized S–H nanocomposite barrier coating is consistent with the Ca-test result and can be attributed to the density

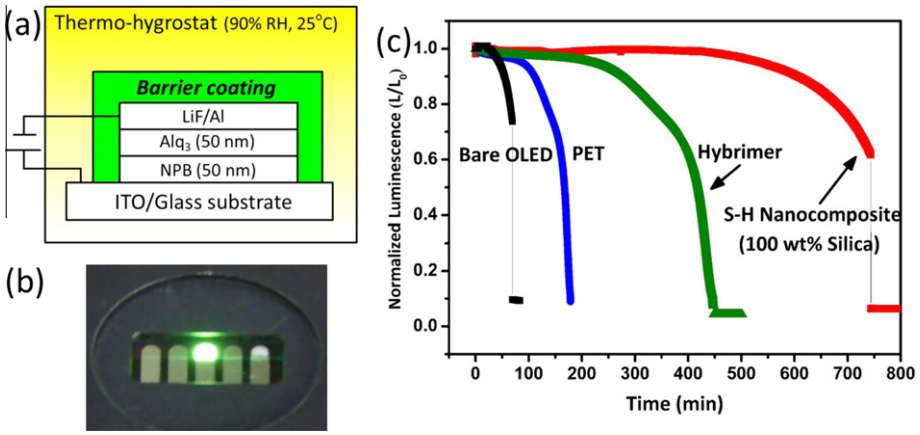

Fig. 6. (a) OLED device structure and test setup for lifetime measurement; (b) Luminescence image of an encapsulated OLED; (c) Measured lifetime of OLED encapsulated with a bare PET film, a neat hybrimer coating and an optimized S–H nanocomposite barrier coating (100 wt% silica content). Plots of normalized luminescence (L/L_0) vs. time.

of the extended tortuous diffusive path for moisture penetrants.

4. Conclusion

In summary, we report a silica nanoparticle-embedded hybrid (S–H) nanocomposite which can be used as an effective moisture barrier coating for transparent OLED encapsulation. We used a sol–gel synthesized organic/inorganic hybrid material (hybrimer) as the matrix and Nanopox® E600 as the filler reinforcement which can make tortuous diffusive paths for moisture penetrants. The S–H nanocomposite even with a high silica content (100 wt%) shows excellent coating quality as well as dispersion morphology, and also high optical transparency. The S–H nanocomposite barrier coating exhibits a single layer WVTR of 0.24 g/m^2 day (Ca-test), and, consistently, demonstrates a significantly extended OLED lifetime.

Acknowledgments

This work is financially supported by The Ministry of Knowledge Economy (MKE) and Korea Institute for Advancement in Technology (KIAT) through the Workforce Development Program in Strategic Technology.

Appendix A. Supplementary data

Supplementary data associated with this article can be found, in the online version, at doi:10.1016/j.orgel.2011.09.008.

References

[1] (a) H. Ito, W. Oka, H. Goto, H. Umeda, Jpn. J. Appl. Phys. 45 (2006) 4325;
(b) J.-W. Park, Y. Kim, H. Lim, C.M. Bae, I. Kim, S. Ando, C.-S. Ha, Mat. Res. Soc. Symp. Proc. (2004) 814;
(c) K.R. Sarma, J. Roush, J. Schmidt, C. Chanley, S. Dodd, Proc. ASID 06 (2006) 337.
[2] (a) H. Aziz, Z. Popovic, S. Xie, A.M. Hor, N.X. Hu, C. Tripp, G. Xu, Appl. Phys. Lett. 72 (1998) 756;
(b) P.E. Burrows, V. Bulovic, S.R. Forrest, L.S. Saposhak, D.M. McCarty, M.E. Thompson, Appl. Phys. Lett. 65 (1994) 2922;
[c] M.S. Xu, J.B. Xu, H.Z. Chen, M. Wang, J. Phys. D Appl. Phys. 37 (2004) 218.
[3] (a) A.S. da Silva Sobrinho, M. Latreche, G. Czeremuszkin, J.E. Klemberg-Sapieha, M.R. Wertheimer, J. Vac. Sci. Technol. A. 16 (1998) 3190;
(b) G. Nisato, P.C.P. Bouten, P.J. Slikkerveer, W.D. Bennett, G.L. Graff, N. Rutherford, L. Wiess, Proc. Asia Display (2001) 1435–1438;
[c] E.H. Song, Y.W. Park, J.H. Choi, T.H. Park, J.W. Jeong, H.J. Choi, B.K. Ju, Rev. Sci. Instrum. 82 (2011) 054702.
[4] (a) P.F. Carcia, R.S. McLean, M.H. Reilly, M.D. Groner, S.M. George, Appl. Phys. Lett. 89 (2006) 031915;
(b) J.H. Choi, Y.-M. Kim, Y.-W. Park, T.-H. Park, J.-W. Jeong, H.-J. Choi, E.-H. Song, J.-W. Lee, C.-H. Kim, B.-K. Ju, Nanotechnology 21 (2010) 475203;
(c) J.-Y. Liao, P.-C. Liu, Y.-H. Yeh, M.-R. Tseng, Proc. SPIE 6655 (2007) 66551O–1.
[5] (a) G.L. Graff, R.E. Wiiliford, P.E. Burrows, J. Appl. Phys 96 (2004) 1840;
(b) B. Singh, J. Bouchet, G. Rochat, Y. Leterrier, J.-A.E. Manson, P. Fayet, Surf. Coat. Tech. 201 (2007) 7107.
[6] (a) Y. Zhong, D. Janes, Y. Zheng, M. Hetzer, D.D. Kee, Polym. Eng. Sci. 2007, DOI:10.1002/pen.20792;
(b) K.S. Triantafyllidis, P.C. LeBaron, I. Park, T.J. Pinnavaia, Chem. Mater. 18 (2006) 4393;
(c) T.J. Pinnavaia, G.W. Beall, Polymer-clay nanocomposites, Wiley, 2000.
[7] R.K. Bharadwaj, Macromolecules 34 (2001) 9189.
[8] (a) K.H. Jung, J.Y. Bae, S.J. Park, S. Yoo, B.-S. Bae, J. Mater. Chem. 21 (2011) 1977;
(b) S.J. Park, K.H. Jung, C. Yun, H. Cho, B.-S. Bae, S. Yoo, IDW Proc. 2010;
[c] Y.C. Han, C. Jang, K.J. Kim, K.C. Choi, K.H. Jung, B.-S. Bae, Org. Electron., 2011, 12, 609.
[9] (a) K.H. Jung, B.S. Bae, J. Appl. Polym. Sci. 108 (2008) 3169;
(b) S.C. Yang, J.-S. Kim, J. Jin, S.-Y. Kwak, B.-S. Bae, J. Appl. Polym. Sci. 117 (2010) 2140.
[10] (a) M.E. Mackay, A. Tuteja, P.M. Duxbury, C.J. Hawker, B.V. Horn, Z. Guan, G. Chen, R.S. Krishnan, Science 311 (2006) 1740;
(b) A.C. Balazs, T. Emrick, T.P. Russell, Science 314 (2006) 1107.
[11] J.B. Hooper, K.S. Schweizer, Macromolecules 39 (2006) 5133.